Tobias Losher

Thomas Kleiner*

Simon Hill

Nadin Sarajlic

Sebastian Rehfeldt

Harald Klein

Comparison of the Generalized Species Transfer Model with a Two-Field Approach for Interfacial Mass Transfer

Two different approaches can be applied to calculate the mass transfer in a two-phase system using computational fluid dynamics and the volume-of-fluid method, single-field and two-field approaches. The used method affects the stability of the calculation as well as the accuracy of the result. Two volume-of-fluid-based approaches, namely, the generalized continuous species transfer model, a single-field approach, and a two-field approach are compared. The models are implemented in the OpenFOAM® framework and validated in a 1D test case. Although both approaches show great agreement with the analytical solution for large time steps, numerical instabilities of the two-field model are revealed with a reduced time step size, which leads to false results.

1 Introduction

The interfacial mass transfer in a multicomponent mixture is crucial in many industrial processes, e.g., absorption/desorption, distillation, or condensation of a mixture [1]. A fundamental understanding of this phenomenon is essential to improve said processes. However, findings obtained from experimental investigations are often limited to particular conditions or mixtures. Therefore, a commonly used method to get a universal tool for process optimization is modeling by computational fluid dynamics (CFD).

Two different approaches for interfacial mass transfer based on the volume-of-fluid (VoF) method can be found in literature: single-field and two-field approaches. Deising et al. [2] present a short comparison of both approaches. The most important aspects are reproduced here. As there are fewer equations to solve in single-field approaches, the computational effort for the mass transfer calculation is lower compared to a two-field approach. On the other hand, in single-field models, there is no consistent concept to calculate the local Sherwood number quantitatively, since the concentrations are given in the volume-averaged form. Concentration gradients can be withdrawn directly within the bulk phases. In cells containing the phase boundary, the concentrations need to be separated prior to gradient extraction.

In two-field approaches, both phases are treated separately so that concentrations as well as concentration gradients are available. Therefore, the local Sherwood number can be withdrawn directly from each field. Drawbacks of the two-field approach are numerical instabilities caused by small cells. Furthermore, the type of VoF method used is the main aspect for

the election of an appropriate mass transfer model [2]. If the advection of the VoF quantity that is employed to distinguish the phases, e.g., the volumetric phase fraction, does not coincide with the advection of molar concentration, an artificial mass transfer across the interface is induced. To perform investigations independent of this criterion, the interface is assumed stagnant in this work and no advection of the volumetric phase fraction is calculated.

In the following, a short summary of successfully implemented single-field and two-field models is presented. It should be noted that many approaches for the description of interfacial mass transfer can be found in literature [3–6]. However, these approaches rely on model parameters, like mass transfer coefficient on the gas and/or liquid side or film thickness, as compared to the regarded models in this work and thus are not further discussed. A detailed summary of published approaches for interfacial mass transfer calculation can be found in the work of Deising et al. [2].

In the context of CO_2 capture, Haroun et al. [7, 8] developed a single-field model to simulate the absorption in gas-liquid flows on structured packings. To describe the interfacial mass transfer, the molar concentrations at the interface are set to equilibrium using Henry's law, and a continuity equation for the molar flux is applied. The continuous species transfer

Tobias Losher, Thomas Kleiner, Simon Hill, Nadin Sarajlic, Dr.-Ing. Sebastian Rehfeldt, Prof. Dr.-Ing. Harald Klein, Thomas.Kleiner@tum.de
Technical University of Munich, Department of Mechanical Engineering, Institute of Plant and Process Technology, Boltzmannstrasse 15, 85748 Garching, Germany.

(CST) model published by Marschall et al. [9] is based on a similar approach. At the interface, the molar concentrations are set to equilibrium by applying Henry's law. Starting from the conservation equations for an arbitrary chemical species, a single-field model is derived by using the conditional volume-averaging technique [10]. Later, Deising et al. [2] combined the models presented by Marschall et al. [9] and Haroun et al. [7, 8]. Within their work, they derive an enhanced CST model.

Hill et al. [11] expanded the CST model to a more general formulation, the generalized species transfer (GCST) model. While the CST model applies Henry's law for the phase equilibrium calculations, the GCST model calculates the phase equilibrium using the relative volatility A_{12}[1]. The models presented so far describe mass transfer based on a single-field formulation. Fleckenstein and Bothe [12] present a different approach. They calculate mass transfer using a two-field model, i.e., each phase is described by a separate concentration field which is extended into the respective other phase with a value of zero. The interfacial coupling is performed through a source term that is added to one phase and subtracted from the other. Rieks and Kenig [13] propose a similar approach. They combine the two-field concentration balance derived by Fleckenstein and Bothe [12] with an approach based on the work of Sáenz et al. [14] to calculate the interfacial source term.

The model used to calculate the interfacial mass transfer can affect the accuracy of the result as well as the stability of the calculation, thus, the choice of an appropriate approach is vital. In this article, the GCST model by Hill et al. [11] is compared with a two-field model based on the work of Rieks and Kenig [13]. Therefore, for the first time, both approaches are implemented in the OpenFOAM® framework and validated in the same 1D test case.

2 Mathematical Formulation

In the considered calculations, no momentum balance is solved. To distinguish the liquid and the vapor phase, an approach based on the VoF method is applied. The volumetric phase fraction γ is calculated by dividing the liquid volume V_L in the cell by the total cell volume V.

$$\gamma = \frac{V_L}{V} \tag{1}$$

In the following, quantities without further indexing of the phase are valid throughout the entire domain. Variables indicated with L (liquid) or V (vapor) represent either phasic-averaged values in the GCST model or variables limited to the respective phase in the two-field formulation. The lower boiling component of a binary mixture is indicated with an index 1, while variables related to the higher boiling component carry an index 2.

As the mole fraction of the lower boiling component calculated in the GCST model is valid throughout the entire domain, the used variable x_1 has no indication referring to the phase. In

contrast, the two-field model determines two mole fractions for the lower boiling component, one for each phase. Consequently, the used variables are written as $x_{1,k}$ where k indicates the liquid (L) or the vapor (V) phase, respectively. As only binary mixtures are considered, the diffusion coefficients $D_{k,12}$ and $D_{k,21}$ are equal so that subscripts indicating the components are omitted.

2.1 GCST Model

Hill et al. [11] derived the GCST model from the CST model [9] for the optimization of a distillation column. The mole fraction x_1 of the lower boiling component is calculated with the single-field formulation.

$$\frac{\partial}{\partial t}(c\,x_1) + \nabla(\mathbf{U}\,c\,x_1) = \nabla\left[\gamma D_L c_L \nabla\left(x_1 \frac{\gamma c_L + (1-\gamma)c_V}{\gamma c_L + K_1(1-\gamma)c_V}\right)\right]$$
$$+ \nabla\left[(1-\gamma)D_V c_V \nabla\left(x_1 K_1 \frac{\gamma c_L + (1-\gamma)c_V}{\gamma c_L + K_1(1-\gamma)c_V}\right)\right] \tag{2}$$

Here, c is the molar concentration, K is the equilibrium ration, $\mathbf{U}$ is the velocity vector, and D_k is the diffusion coefficient in phase k. To arrive at the single-field formulation given in Eq. (2), the conditional volume-averaging technique [10] is applied to local instantaneous transport equations of the molar fraction in both phases. For the closure of the resulting system of equations, the equilibrium condition is used. This is possible, if the following assumption of Marschall et al. [9] holds true: the local mole fraction at the interface is assumed to equal the volume-averaged mole fraction in the corresponding phase [11]. This results in a strong dependence between the accuracy of the model and the spatial resolution of the interface. A detailed derivation of the GCST model can be found in the work of Hill et al. [11].

Furthermore, Eq. (2) requires the equilibrium ratio K_1 of the lower boiling component as an input. This quantity is calculated with the relative volatility A_{12} and the mole fraction of the lower boiling component in the liquid phase. It should be noted that the assumption of a constant relative volatility limits the model to ideal mixtures.

$$K_1 = \frac{A_{12}}{1 + (A_{12}-1)(x_{1,L})^o} \tag{3}$$

As the liquid mole fraction $x_{1,L}$ is unknown, its value $(x_{1,L})^o$ of the previous time step is applied to estimate K_1. To determine $(x_{1,L})^o$, the following equation is solved:

$$(x_1)^o[(\gamma)^o c_L + (1-(\gamma)^o)c_V] =$$
$$(\gamma)^o c_L (x_{1,L})^o + (1-(\gamma)^o)c_V \frac{A_{12}(x_{1,L})^o}{1 + (A_{12}-1)(x_{1,L})^o} \tag{4}$$

Due to its polynomial character, Eq. (4) yields two solutions. As negative values for the mole fraction are not plausible, the positive solution is chosen.

2.2 Two-Field Model

The two-field model is based on the work of Rieks and Kenig [13]. In this approach, each phase is described separately. Therefore, the used variables were limited to the related phase with appropriate indicator functions ε_k and extended into the respective other phase with a value of zero. Then, the coupling at the interface is performed with an equilibrium condition. The definition of the indicator functions ε_k for each phase reads:

$$\varepsilon_k = \begin{cases} 1, & \text{in phase } k \\ 0, & \text{elsewhere} \end{cases} \tag{5}$$

Analogously, the function β is introduced to identify the interface.

$$\beta = \begin{cases} 1, & \text{at the interface}; \gamma \in [0.001; 0.999] \\ 0, & \text{elsewhere} \end{cases} \tag{6}$$

The mass transport equations solved in this model are based on the ones derived by Fleckenstein and Bothe [12]:

$$\frac{\partial}{\partial t}\left(\varepsilon_L c_L x_{1,L}\right) + \nabla\left(\varepsilon_L \mathbf{U} c_L x_{1,L}\right) - \nabla\left(\varepsilon_L D_L c_L \nabla x_{1,L}\right) = -S_{x_1} \tag{7}$$

$$\frac{\partial}{\partial t}\left(\varepsilon_V c_V x_{1,V}\right) + \nabla\left(\varepsilon_V \mathbf{U} c_V x_{1,V}\right) - \nabla\left(\varepsilon_V D_V c_V \nabla x_{1,V}\right) = S_{x_1} \tag{8}$$

In both equations, ε_k limits the convective and diffusive mass transfer to the related phase k. A source term S_{x_1} is added in one equation and withdrawn in the other to describe the mass transfer across the interface. The use of only one source term for both equations ensures the conservation of mass during the mass transfer across the interface. Due to the addition of S_{x_1}, the mole fractions are forced to the corresponding equilibrium values at the interface. This approach is based on the work of Sáenz et al. [14]. The definition of the equilibrium ratio

$$K_1 = \frac{x_{1,V}^*}{x_{1,L}^*} \tag{9}$$

is employed to estimate the equilibrium mole fraction $x_{1,V}^*$ in the vapor phase. Solving Eq. (9) for the equilibrium value $x_{1,V}^*$ that belongs to the liquid mole fraction $x_{1,L}$ at the interface, the relation for the source term S_{x_1} reads:

$$S_{x_1} = \beta\left(\frac{K_1 x_{1,L} - x_{1,V}}{\Delta t}\right) c_V \tag{10}$$

The source term is only relevant at the interface. This is achieved through the multiplication with the indicator function β. Due to a strongly coupled relation between the source term S_{x_1} (Eq. (10)) and the mole fractions $x_{1,L}$ and $x_{1,V}$ (Eqs. (7) and (8)), the calculation of the mass transport is carried out iteratively. During the iteration j, Eqs. (7) and (8) are solved for $x_{1,L}^j$ and $x_{1,V}^j$ using the source term $S_{x_1}^{j-1}$. Afterwards, the source term is updated to $S_{x_1}^j$ by Eq. (10) and the updated mole frac-

tions $x_{1,L}^j$ and $x_{1,V}^j$. This iteration is carried out until the residuum of S_{x_1} is smaller than the desired tolerance.

For the model comparison, the mole fractions $x_{1,L}$ and $x_{1,V}$ of the lower boiling component are summarized to a variable x_1 valid throughout the entire domain. This is not implemented in the mathematical model itself.

$$x_1 = \begin{cases} x_{1,L}, & \text{if } \varepsilon_L = 1 \\ x_{1,V}, & \text{if } \varepsilon_V = 1 \end{cases} \tag{11}$$

Similarly, an overall molar flux Φ_1 of the lower boiling component is introduced:

$$\Phi_1 = \begin{cases} \Phi_{1,L}, & \text{if } \varepsilon_L = 1 \\ \Phi_{1,V}, & \text{if } \varepsilon_V = 1 \end{cases} \tag{12}$$

The figures presented in this work show the summarized variables x_1 and Φ_1. As a consequence, only valid parts of the phase-related quantities are plotted for the two-field model, while regions are neglected where the mole fractions $x_{1,k}$ and the molar fluxes $\Phi_{1,k}$ are set to zero.

3 Comparison of the GCST Model and the Two-Field Model

In this section, the 1D test case is introduced that is used to compare the GCST and the two-field model. Furthermore, the resulting mole fraction and molar flux profiles are discussed and validated using an analytical solution.

3.1 Setup of the 1D Test Case

Hill et al. [11] introduce a 1D test case to determine the grid independence of their model. To compare the transport models, the same setup is employed here. This allows the analytical calculation of the mole fraction and consequently a meaningful validation of the numerical models. Fig. 1 illustrates the case setup and the boundary conditions used for the simulations.
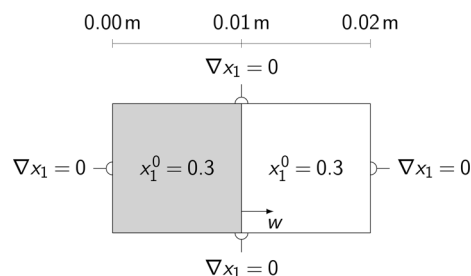

Figure 1. Setup of the 1D test case used to compare the GCST model and the two-field approach.

Liquid (marked with a gray background) and vapor phase are assumed stagnant. As starting conditions, the mole fractions are set to $x_1^0 = 0.3$. On all boundaries zero gradient conditions $\nabla x_1 = 0$ are imposed. In the GCST model, the relative volatility is assigned a constant value of $A_{12} = 4.2$. Under these

conditions, Eq. (3) yields an equilibrium ratio of K_1 = 2.14, which is used in the two-field formulation and is also considered to be constant. To ensure a sufficient spatial discretization, the domain is divided into 1001 evenly spaced cells in w-direction as both models provide a net independent solution for this grid resolution. Thereof, the interface is resolved with a single cell and each phase is resolved with 500 cells, respectively. The other directions are not resolved.

3.2 Analytical Solution

For the model validation, the numerically calculated vapor mole fraction $x_{1,V}$ and the molar flux $\Phi_{1,V}$ in the vapor phase were compared with an analytical solution. If the mole fraction $x_{1,L}$ remains constant, $x_{1,V}$ can be calculated analytically using the approach of a semi-infinite body where the surface concentration at the interface is fixed [15]. The analytical solution reads

$$x_{1,V}(w, t) = K_1 x_{1,L}^0 + \left(x_{1,V}^0 - K_1 x_{1,L}^0\right) \mathrm{erf}\left(\frac{w}{2\sqrt{D_V t}}\right) \qquad (13)$$

To calculate $\Phi_{1,V}$ under the mentioned conditions, the analogy of heat and mass transfer is employed. Polifke and Kopitz [16] give an analytical solution for the heat flux into:

$$\Phi_{1,V}(w, t) = -c\sqrt{\frac{D_V}{\pi t}}$$
$$\times \left(x_{1,V}^0 - K_1 x_{1,L}^0\right)\exp\left(-\left(\frac{w}{2\sqrt{D_V t}}\right)^2\right) \qquad (14)$$

To fulfill the condition of an approximately constant liquid mole fraction, the following constraints have to be met:

$$c_L D_L \gg c_V D_V \quad \text{and} \quad c_L \gg c_V \qquad (15)$$

3.3 Model Comparison

To meet the conditions stated in Eq. (15), the diffusion coefficients are set to $D_L = 10^{-4}\,\mathrm{m^2 s^{-1}}$ and $D_V = 10^{-6}\,\mathrm{m^2 s^{-1}}$ and the molar concentrations are set to $c_L = 100\,\mathrm{mol\,m^{-3}}$ and $c_V = 1\,\mathrm{mol\,m^{-3}}$. Fig. 2 compares the mole fraction x_1 and the molar flux Φ_1 of the presented models at a time of t = 2.5 s. The simulation was performed with a time step size $\Delta t = 10^{-3}$ s for the GCST model while the two-field formulation was discretized with $\Delta t = 10^{-2}$ s.

Both simulations show great agreement with the analytical solution. Under these conditions, the GCST model and the two-field model yield the same mole fraction and molar flux profiles. Therefore, it is sufficient to discuss the simulation result of only one model. The magnified view of the liquid mole fraction shows a slight decrease of x_1 in the liquid phase with respect to the initial mole fraction x_1^0. As the change in the liquid mole fraction is one order of magnitude smaller than x_1^0, the approximation of a fixed interfacial concentration is still justified.

The mole fraction profiles in both phases are strictly monotonously falling towards the vapor bulk phase. This complies with the expected mass transfer from liquid to vapor. Looking at the molar flux, it should be noted that the molar fluxes of liquid and vapor phase coincide at the interface. Consequently, a conservation of mass during the transfer across the interface is given.

If the two-field simulation is discretized with a time step size of $\Delta t = 10^{-3}$ s, the calculation yields the profiles displayed in Fig. 3.

Although the numerically determined molar flux in the vapor phase stands in excellent agreement with the analytical solution, the molar flux in the liquid phase differs from the expected profile. To get steady mass transport from one bulk phase to the other, a maximum molar flux at the interface would be necessary. The magnified view of the mole fraction profile displays an inflection point near the interface. As the
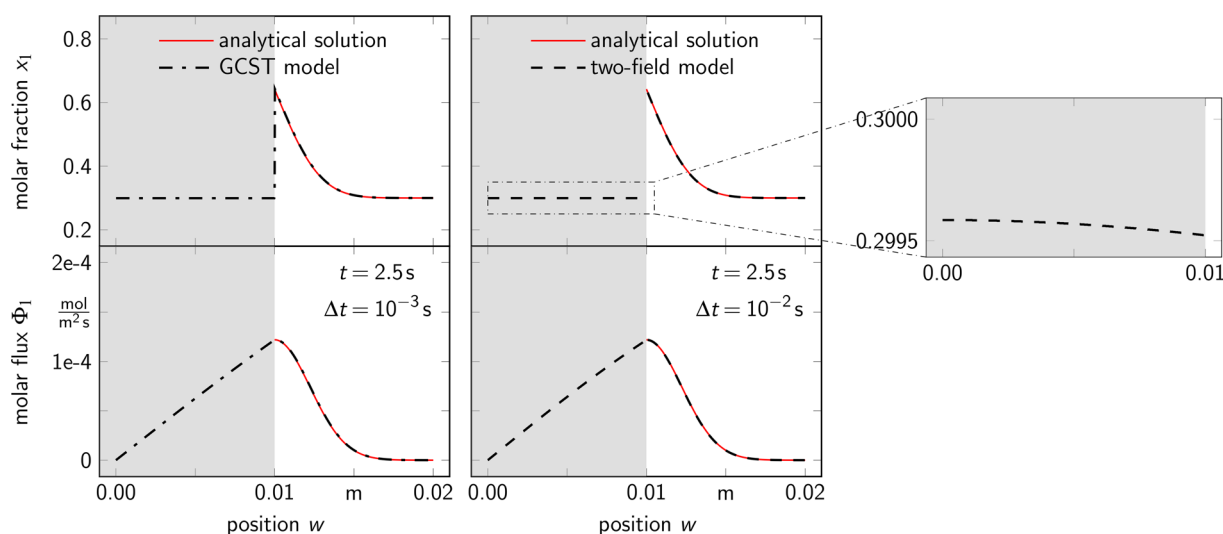

Figure 2. Comparison of the GCST model and the two-field model in the 1D test case, including the analytical solution in the vapor phase.
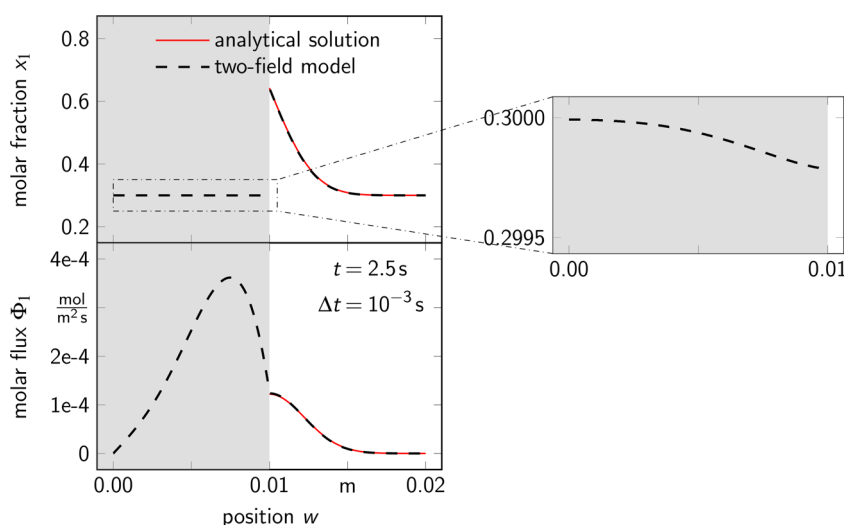
Figure 3. Results of the two-field model with a small time step simulated in the 1D test case, including the analytical solution in the vapor phase.

molar flux Φ_1 is proportional to the gradient of the mole fraction ∇x_1, this causes a maximum in the molar flux profile. A reason for the development of this profile can be found in Eq. (10), the definition of the source term. S_{x_1} is used to set the vapor mole fraction $x_{1,V}$ to the equilibrium value $x_{1,V}^* = K_1 x_{1,L}$ within one time step. Consequently, the source term increases with decreasing time step size. This can have a negative impact on the numerical stability of the calculation.

In the present case, the initial mole fraction is set to $x_1^0 = 0.3$, a state far from equilibrium. The small time step size, the high diffusion coefficient, and the chosen initial mole fractions lead to a large initial source term and result in an overcorrection of the interfacial liquid mole fraction to values lower than the actual equilibrium value. Although the liquid mole fraction at the interface is corrected during the following time steps, the error produced in the first time steps is only counteracted within the interface cell. Analogously, the large molar flux calculated in the first time steps is transported into the bulk phase. Therefore, it is assumed that the origin of the unexpected concentration profile in the liquid phase lies in the error produced in the first time steps.

3.4 Case Adaption

To investigate the made assumption of the previous subsection, the case setup is adapted to a 2D test case with a stationary solution, in which mass transfer across the interface is also only driven by diffusion. The setup is illustrated in Fig. 4.

Analogously to the 1D test case, the position of the interface stays the same throughout the simulation. The initial mole fractions are set to $x_1^0 = 0$ throughout the entire domain. Due to a velocity of $U_v = 2 \, \text{m s}^{-1}$ in vertical direction, imposed on the lower boundary, a constant liquid and vapor mole fraction of $x_1^0 = 0.3$ is transported into the corresponding phases, respectively. The 2D test case contains the previous 1D test case if the flow is followed in a Lagrangian perspective.

To get comparable results to the 1D test case, mass transfer has to take place for the same period of time as before. Therefore, the v-coordinate position of the presented results depending on the flow velocity U_v and the residence time τ was chosen. Multiplying the imposed velocity in v-direction $U_v = 2 \, \text{m s}^{-1}$ with a residence time τ that equals the simulation time of the 1D case, the desired length yields $L = U_v \tau = 5 \, \text{m}$. It should be noted that there is diffusive mass transport in flow direction that is neglected. With a velocity of $U_v = 2 \, \text{m s}^{-1}$ the convective transport predominates the diffusion in flow direction so that this simplification is justified. Similar to the 1D case, the domain is divided into 1001 evenly spaced cells in w-direction. To ensure grid independence, a spatial discretization of $\Delta v = 0.03 \, \text{m}$ is applied in v-direction. The third direction in space is not resolved.
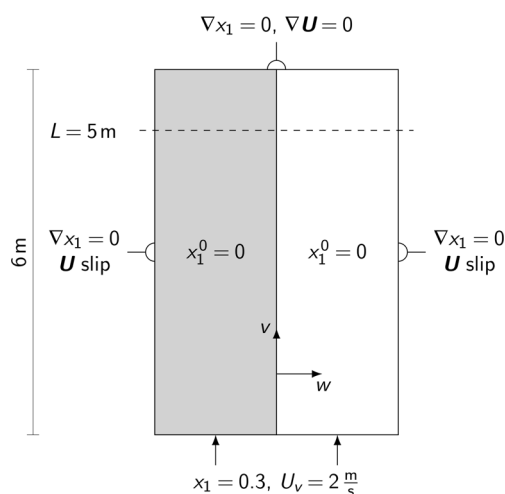

Figure 4. Setup of the 2D case to validate the two-field method.

After a time of $t = 10 \, \text{s}$ steady state is reached. Fig. 5 shows the calculated results at the length L. As in the other simulations, the numerical results stand in great agreement with the analytical solution. In addition, the unphysical behavior found in Fig. 3 is avoided with the presented approach. If these results are compared to the profiles obtained by the GCST model simulation, no difference can be determined.

Due to the convection in v-direction, the error produced in the first time steps flows out of the simulation domain. To illustrate this behavior, the liquid molar flux $\Phi_{1,L}$ at the interface, i.e., at $w = 0.01 \, \text{m}$, is plotted against the v-coordinate for $t = 2.5 \, \text{s}$, which is given in Fig. 6.

The molar flux $\Phi_{1,L}$ has its maximum at $v \approx 5 \, \text{m}$, while the amplitude of the oscillation decreases towards the inlet. After $t = 2.5 \, \text{s}$ the mole fraction imposed on the lower boundary has been transported 5 m into the domain due to convection. Consequently, the maximum of $\Phi_{1,L}$ at $v \approx 5 \, \text{m}$ corresponds to the
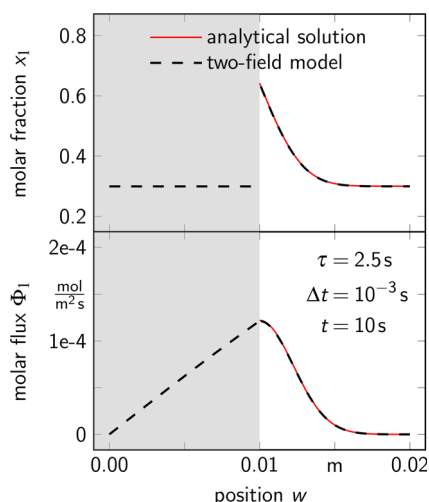
Figure 5. Results of the two-field model with a small time step size, simulated in the 2D case, including the analytical solution in the vapor phase.
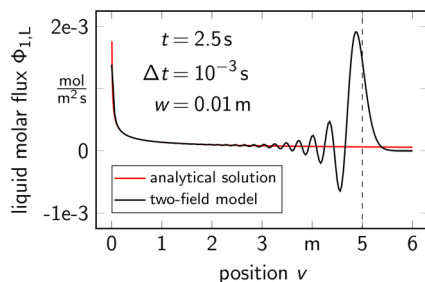

Figure 6. Profile of the interfacial liquid molar flux $\Phi_{1,L}$ in flow direction.

first time steps of the simulation. At the inlet, the iterative calculation of the source term S_{x_1} is repeated permanently. Therefore, the high values due to the initial overshooting decline at this position until a steady value is reached, and the imposed convection carries fluctuations of the molar flux out of the simulation domain.

The numerical instabilities decrease as the difference between the interfacial mole fractions and the corresponding equilibrium values decrease. In contrast to the 1D case, the numerical instabilities at the first time steps have no influence on the desired simulation results. Therefore, the false concentration profile found in the 1D test case can be attributed to the produced errors of the initial time steps.

4 Conclusion

Two different approaches to calculate the interfacial mass transfer in a binary mixture are compared with the main focus on the impact of the temporal discretization. The first concept, termed GCST model [11], determines the mole fraction in both phases with a single-field formulation. This approach is contrasted with a two-field model similar to the work of Rieks and Kenig [13].

The models are implemented in the OpenFOAM® framework and validated against an analytical solution in a 1D test case with a stagnant interface. Initially, the simulation results of the GCST models are compared with a temporal discretization of $\Delta t = 10^{-3}$ s and the two-field formulation with a time step size of $\Delta t = 10^{-2}$ s. Both approaches stand in excellent agreement with the analytical solution and their results coincide perfectly. In a second step, the time step size used in the two-field model to $\Delta t = 10^{-3}$ s is reduced This results in false mole fraction and molar flux profiles, which is due to a large source term at the interface in the first time steps. For further investigation, a 2D case with stationary convection perpendicular to the interfacial mass transfer is introduced for the two-field simulation. The profiles arising from this calculation show great agreement with the analytical solution and coincide perfectly with the results of the GCST model.

Both methods are promising approaches for the modeling of interfacial mass transfer in binary mixtures and provide results that stand in excellent agreement with the analytical solution of a 1D problem. In addition to the known differences between single-field and two-field approaches [2], this work reveals the numerical instability of the presented two-field model due to small time step sizes. As industrially relevant simulations require a fine spatial and temporal discretization due to their complexity, numerical problems caused by large source terms can complicate the calculation if the two-field approach is used. The transformation into a steady-state problem or a reduction of the amount of species that crosses the interface counteract the revealed problem. The latter can be achieved through initial conditions near equilibrium state. These aspects should be taken into account, when selecting an appropriate mass transfer model.

Symbols used

A_{12}	[–]	relative volatility
c	[mol m^{-3}]	molar concentration
D	[m^{2}s^{-1}]	diffusion coefficient
K	[–]	equilibrium ratio
L	[m]	length
S_{x_1}	[mol m^{-3}s^{-1}]	volumetric molar source term
t	[s]	time
Δt	[s]	time step size
U	[m s^{-1}]	velocity
U_v	[m s^{-1}]	velocity in v-direction
V	[m^3]	volume
v, w	[m]	coordinate axes
Δv	[m]	spatial discretization in v-direction
x	[–]	mole fraction

Greek letters

β	[–]	indicator function for the interface
γ	[–]	volumetric phase fraction
ε	[–]	indicator function for the phases
τ	[s]	residence time
Φ	[mol m^{-2}s^{-1}]	molar flux

Sub- and superscripts

*	equilibrium value
0	initial state
1	lower boiling component
2	higher boiling component
j	iteration variable
k	arbitrary phase, $k \in \{L,V\}$
L	liquid
o	old value
V	vapor

Abbreviations

CFD	computational fluid dynamics
CST	continuous species transfer
GCST	generalized species transfer
VoF	volume-of-fluid

References

[1] J. G. Stichlmair, J. R. Fair, *Distillation: Principles and Practice*, 1st ed., Wiley-VCH, Weinheim **1998**.

[2] D. Deising, H. Marschall, D. Bothe, *Chem. Eng. Sci.* **2016**, *139*, 173–195. DOI: https://doi.org/10.1016/j.ces.2015.06.021

[3] M. Haghshenas Fard, M. Zivdar, R. Rahimi, M. Nasr Esfahany, A. Afacan, K. Nandakumar, K. T. Chuang, *Chem. Eng. Technol.* **2007**, *30 (7)*, 854–861. DOI: https://doi.org/10.1002/ceat.200700011

[4] J. Chen, C. Liu, X. Yuan, G. Yu, *Chin. J. Chem. Eng.* **2009**, *17 (3)*, 381–388. DOI: https://doi.org/10.1016/S1004-9541(08)60220-7

[5] Y. Y. Xu, S. Paschke, J.-U. Repke, J. Q. Yuan, G. Wozny, *Chem. Eng. Technol.* **2009**, *32 (8)*, 1227–1235. DOI: https://doi.org/10.1002/ceat.200900099

[6] D. Sebastia-Saez, S. Gu, P. Ranganathan, K. Papadikis, *Int. J. Greenhouse Gas Control* **2013**, *19*, 492–502. DOI: https://doi.org/10.1016/j.ijggc.2013.10.013

[7] Y. Haroun, D. Legendre, L. Raynal, *Chem. Eng. Sci.* **2010**, *65 (1)*, 351–356. DOI: https://doi.org/10.1016/j.ces.2009.07.018

[8] Y. Haroun, D. Legendre, L. Raynal, *Chem. Eng. Sci.* **2010**, *65 (10)*, 2896–2909. DOI: https://doi.org/10.1016/j.ces.2010.01.012

[9] H. Marschall, K. Hinterberger, C. Schüler, F. Habla, O. Hinrichsen, *Chem. Eng. Sci.* **2012**, *78*, 111–127. DOI: https://doi.org/10.1016/j.ces.2012.02.034

[10] C. Dopazo, *J. Fluid Mech.* **1977**, *81 (3)*, 433–438. DOI: https://doi.org/10.1017/S0022112077002158

[11] S. Hill, T. Acher, R. Hoffmann, J. Ferstl, D. Deising, H. Marschall, S. Rehfeldt, H. Klein, *Chem. Eng. Trans.* **2018**, *69*, 337–342. DOI: https://doi.org/10.3303/cet1869057

[12] S. Fleckenstein, D. Bothe, *J. Comput. Phys.* **2015**, *301*, 35–58. DOI: https://doi.org/10.1016/j.jcp.2015.08.011

[13] S. Rieks, E. Y. Kenig, *Chem. Eng. Sci.* **2018**, *176*, 367–376. DOI: https://doi.org/10.1016/j.ces.2017.10.040

[14] P. J. Sáenz, P. Valluri, K. Sefiane, G. Karapetsas, O. K. Matar, *Phys. Fluids* **2014**, *26 (2)*, 024114. DOI: https://doi.org/10.1063/1.4866770

[15] *Fundamentals of Momentum, Heat, and Mass Transfer* (Eds: J. R. Welty, C. E. Wicks, R. E. Wilson, G. L. Rorrer), 5th ed., John Wiley & Sons, Hoboken, NJ **2008**.

[16] *Wärmeübertragung: Grundlagen, analytische und numerische Methoden* (Eds: W. Polifke, tJ. Kopitz), 2nd ed., Pearson, Munich **2009**.